Journal of Solid State Chemistry **168,** 175–183 (2002)
doi:10.1006/jssc.2002.9707

TeO_2–WO_3 Glasses: Infrared, XPS and XANES Structural Characterizations

P. Charton,*[,1] L. Gengembre,† and P. Armand*

*LPMC, UMR CNRS 5617, UMII, c.c. 003, Place E. Bataillon, 34095 Montpellier Cedex 5, France; and †Université des Sciences et Technologies de Lille, Laboratoire de Catalyse, CNRS-UPRESA 8010, Bât. C3, 59655 Villeneuve d'Ascq Cedex, France

Received March 14, 2002; in revised form June 24, 2002; accepted July 16, 2002

Transparent $(1-x)TeO_2$–xWO_3 glasses with $0 \le x \le 0.325$ mol were synthesized by the fast quenching technique. Several complementary techniques as infrared, X-ray photoelectron and X-ray absorption spectroscopies were used to approach the structure of these tungsten oxide–tellurite glasses. Special attention was paid to the oxidation state and the coordination state of tungsten atoms. The structural results show that $(1-x)TeO_2$–xWO_3 glasses present characteristic tellurium environments which vary with their chemical composition while tungsten ions always adopt an octahedral configuration. © 2002 Elsevier Science (USA)

Key Words: **oxide glasses; tellurite; tungsten oxide; infrared; X-ray photoelectron spectroscopy; X-ray absorption; XANES; XPS; TeO_2.**

1. INTRODUCTION

The synthesis of glasses with high refractive index values is of great importance in the glass science and the optical industries. Tungsten oxide–tellurite glasses have been obtained showing an extremely high refractive index with low dispersion value, low crystallization ability and good chemical resistance (1, 2). Also, they exhibit good light transmission in the visible and near infrared regions up to 5.5 μm (3). For these reasons, TeO_2–WO_3 glasses have become the subject of several investigations. The glass formation domain has been determined and the thermal parameters examined by several authors (1, 4, 5). Neutron scattering experiments and vibrational spectroscopy studies, especially Raman analysis, were conducted to follow the effect of WO_3 on the structure of tellurite glasses (2, 6–11). On the other hand, no structural characterizations by X-ray absorption (XANES) and X-ray photoelectron (XPS) spectroscopies were undertaken, in our knowledge, on these tungsten-oxide glasses.

Despite many characterizations, the structure of TeO_2–WO_3 glasses is still subject to discussion. Indeed, some authors agree with the evolution of the TeO_4 trigonal bipyramid polyhedra with the increase in WO_3 content (8, 10), while some authors have the opinion that WO_3 does not lead to a Te coordination change (7, 11). The same discussion exists concerning the tungsten coordination sphere, i.e., existence of WO_4 tetrahedra or/and WO_6 octahedra (2, 7, 9).

The purpose of this paper was to approach the structure of glasses obtained in the TeO_2–WO_3 system by several complementary techniques; infrared, X-ray photoelectron and XANES. Special attention was paid to the oxidation state and the coordination state of tungsten atoms.

2. EXPERIMENTAL CONSIDERATIONS

2.1. Sample Preparation

The glass samples were prepared by melting mixtures of analytic grade reagents of α-TeO_2 and γ-WO_3 in an electric furnace heated up to 900°C. The platinum crucible containing the melt was quickly quenched in an ice-cold water bath to avoid crystallization. In order to extend the glass-forming domain and to improve the samples quality (homogeneity), some preparations were quenched in a freezing mixture (−10°C) made of ethanol, ice and NaCl. Indeed, it is the only way to prepare pure TeO_2 glass (12) (13). The amorphous state of each sample was checked by X-ray diffraction. Clear and transparent $(1-x)TeO_2$–xWO_3 glass compositions with $0 \le x \le 0.325$ were synthesized. The color of glasses changes from yellow to light orange depending on composition. Both the homogeneity and the chemical concentration of each glass were checked by electronic microscopy with X-ray analysis. The samples were not subjected to any annealing processes and were used as obtained.

[1] To whom correspondence should be addressed. Fax: +33-4-67-14-42-90. E-mail: pcharton@lpmc.univ-montp2.fr.

0022-4596/02 $35.00

White α-TeO_2 (14) and yellow monoclinic γ-WO_3 (15) compounds are commercial powders (Aldrich, Fluka) with a nominal purity of 99.99%. The tungstates of alkali and alkaline earth metals were prepared by solid state reaction of the carbonate Li_2CO_3 or $BaCO_3$ (commercial products from Aldrich) with γ-WO_3. White $Li_2W_2O_7$ powder with the triclinic symmetry (16) was obtained after 24 h at 700°C. White $BaWO_4$ powder with the tetragonal symmetry was synthesized at 755°C during 3 days (17). Stoichiometric PbO (Fluka) and γ-WO_3 mixture was heated up to 750°C during 3 days to form β-$PbWO_4$ stolzite form (18). X-ray diffraction was used to confirm the crystallized state and the single-phase structure.

2.2. Physical Characterizations

Infrared (IR) transmission measurements were made using a Perkin-Elmer 1600 series FTIR spectrometer from 4000 to 400 cm^{-1} at intervals of 4 cm^{-1}. Measurements were carried out on identical KBr pellets.

Te L_{III} edge X-ray absorption near edge structure (XANES) measurements were carried out on the D44 beam line of the DCI storage ring at LURE (Orsay) working with an electron energy of 1.85 GeV and an average positron current of 250 mA. Room temperature data were collected in transmission mode using two ionization chambers filled with He/Ne mixture. A double crystal Si(111) monochromator was used to obtain a single beam. The harmonic energies were rejected using a grazing incidence mirror (19). The energy steps and the counting times were adjusted to improve data quality. Samples were prepared by grinding and sieving glasses to obtain fine powders with regular grain size of 20 μm. The mass of glass powder has been previously computed to avoid saturation effects and to optimize the signal-to-noise ratio. The powders were then dispersed in ethanol and settled on a microporous membrane to obtain homogenous samples deposits.

W L_{III} and L_I edges XANES spectra were recorded using a Si(311) double crystal monochromator with ionization chambers containing argon. The computed mass of glass was thoroughly mixed with cellulose used as binder and the mixture was pressed in 10-mm diameter pellet.

To compare the XANES spectra, the absorption background subtraction was first carried out using a linear function on the pre-edge region and the spectra then normalized by taking an energy point around 80 eV above the edge.

Measurements of the X-ray photoelectron (XP) core-level spectra were carried out with an ESCALAB-220XL spectrometer. Monochromatic 120 W Al$K\alpha$ X-ray provided the excitation radiation. Under these conditions, the irradiated surface was a 500-μm diameter spot. The working pressure inside the analyzer chamber was about 5×10^{-8} Pa. The dispersif hemispheric-type electron analyzer was set at a band pass energy of 30 eV. In this case, the instrumental resolution taken as the full-width at half-maximum (FWHM) of the Ag_{3d5} photo-peak was 0.75 eV. The C1s peak position corresponding to a hydrocarbon environment (C–C and C–H bonds) was located at 285 eV. The insulator samples were put under a secondary electron flux of weak energy (6 eV) to compensate the charge effects. The powdered samples are pressed on an indium foil and a 2-mm diameter metallic (stainless steel) diaphragm is placed on to favor the charge evacuation. Data processing was done using the commercial ECLIPSE software. The photo-peak area was determined after subtraction of the non-linear spectral background of Shirley type (20). The spectral simulations were based on a Lorentz (30%)–Gaussian (70%) profile.

3. RESULTS

3.1. Infrared Spectroscopy

The infrared transmission spectra of crystalline compounds taken as references are given in Fig. 1a. In the paratellurite α-TeO_2 form, the Te environment consists in distorted trigonal bipyramids (tbp) TeO_4E with C_{2V} point group ($2Te–O_{ax} = 2.12$ Å, $2Te–O_{eq} = 1.88$ Å and E = Te $5s^2$ lone pair (14)). According to Arnaudov *et al.* (21), the sharp band at 770 cm^{-1} corresponds to the symmetric equatorial $(\nu^{s}TeO_2)_{eq}$ vibration, while the broad non-symmetric band at 660 cm^{-1} includes the asymmetric equatorial $(\nu^{as}TeO_2)_{eq}$, the symmetric and asymmetric axial $(\nu^{as}TeO_2)_{ax}$ and $(\nu^{s}TeO_2)_{ax}$ stretching modes of the TeO_4E units.

The room-temperature γ-WO_3 modification, with $P2_1/n$ space group (15), is composed of corner-sharing WO_6 octahedra having large distortion. Its IR spectrum is dominated by a strong and large band centered at about 850 cm^{-1} with two shoulders at 770 and 910 cm^{-1}. $Li_2W_2O_7$ crystallizes in the triclinic space group $P-1$ and is built up of largely distorted WO_6 octahedra and LiO_4 tetrahedra (16). By sharing edges, the WO_6 octahedra form infinite double chains of $(W_2O_7)^{2-}$ extending along the c-axis. Because the tungsten environment is more distorted in $Li_2W_2O_7$ crystalline compound (larger set of distances than in WO_3), we observe more distinctly many bands characterizing the W–O vibrations. This could be explained by a removal of degeneracy for $Li_2W_2O_7$ compared to WO_3.

$BaWO_4$ (17) and β-$PbWO_4$ (18) compounds with the scheelite-like structure belong to the space group $I4_1/a$. In these structures, the W atoms are located at the center of the isolated regular tetrahedra. Their IR spectra show two maxima in the 770–850 cm^{-1} range which agree well with previous works (22).

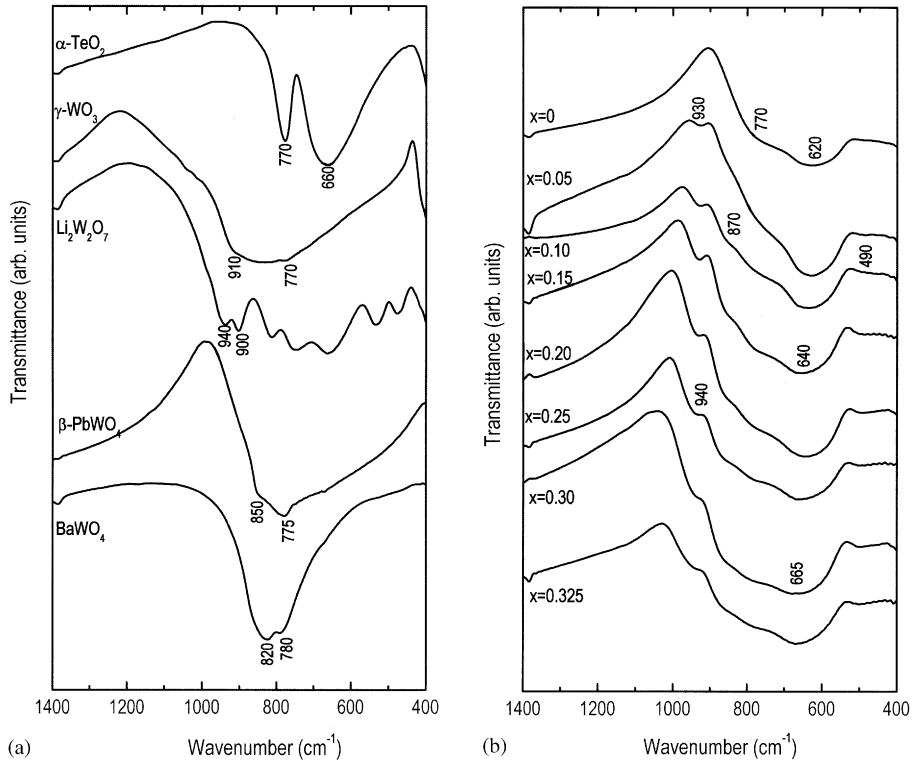

FIG. 1. Infrared spectra of (a) crystallized references and (b) $(1-x)TeO_2$–xWO_3 glasses with $0 \le x \le 0.325$.

IR spectra of $(1-x)TeO_2$–xWO_3 glass samples with various compositions x, Fig. 1b, consist of major bands in the 600–800 cm^{-1} range and a band around 930 cm^{-1}. The typical broadening of the vibration bands due to the glassy state is observed. TeO_2 glass ($x = 0$) IR spectrum is rather similar to α-TeO_2 data. The 620 cm^{-1} major band and the shoulder at about 770 cm^{-1} are, respectively, assigned to symmetrical vibrations of Te–O_{ax} bonds and to symmetric vibrations of Te–O_{eq} bonds of TeO_4E units (23). As the WO_3-content increases, Fig. 1b, the major band shifts from 620 cm^{-1} ($x = 0$) to 665 cm^{-1} ($x = 0.325$). This may be related to the apparition of TeO_3E units concomitant to a reduction in the number of TeO_4E units (24, 25). The 770 cm^{-1} shoulder relative to the existence of TeO_4E units is still present for $x = 0.325$.

The absorption band at 490 cm^{-1} which slightly increases in intensity with WO_3-content is inactive in the IR spectrum of TeO_2 glass ($x = 0$), Fig. 1b. The appearance of this new band shows the direct influence of the WO_3 oxide on the tellurite network. It can be assigned to Te–O–W bridging bonds which would increase the network connectivity. This assignment is made in agreement with the theoretical model for vibrations of mixed bridge bonds containing heavy metal and glass former atoms (26). Then, the formation of Te–O–W bridging bonds is expected because both W and Te atoms have comparable electronegativity and can therefore substitute for each other in bonding with O atoms (11). That is, there is a small fraction of W cations which are incorporated in the glass network.

The 930 cm^{-1} band and the 870 cm^{-1} shoulder are directly connected to W–O vibrations since they are inactive in the IR spectrum of TeO_2 glass. The 870 cm^{-1} shoulder is assigned to W–O–W vibrations (2, 8, 27). Compared to the tungstate references, Fig. 1a, the 930 cm^{-1} band may be assigned to the existence of distorted WO_6 octahedra as encountered in $Li_2W_2O_7$. On the other hand, the IR spectra of K_2WO_4 and Rb_2WO_4 crystalline compounds containing slightly distorted tetrahedra WO_4 present a weak band at around 925 cm^{-1} (28). Thus, from IR spectroscopy the attribution of the 930 cm^{-1} band is difficult.

3.2. *Te L_{III} Edge XANES Spectroscopy*

Figure 2a compares the Te L_{III} edge normalized XANES spectra of $(1-x)TeO_2$–xWO_3 glasses of various compositions with the references α-TeO_2 and Tl_2TeO_3. This latter contains isolated trigonal pyramid TeO_3E units with regular bond length (29). Tl_2TeO_3 as powder was kindly provided by the SPCTS (Limoges, France).

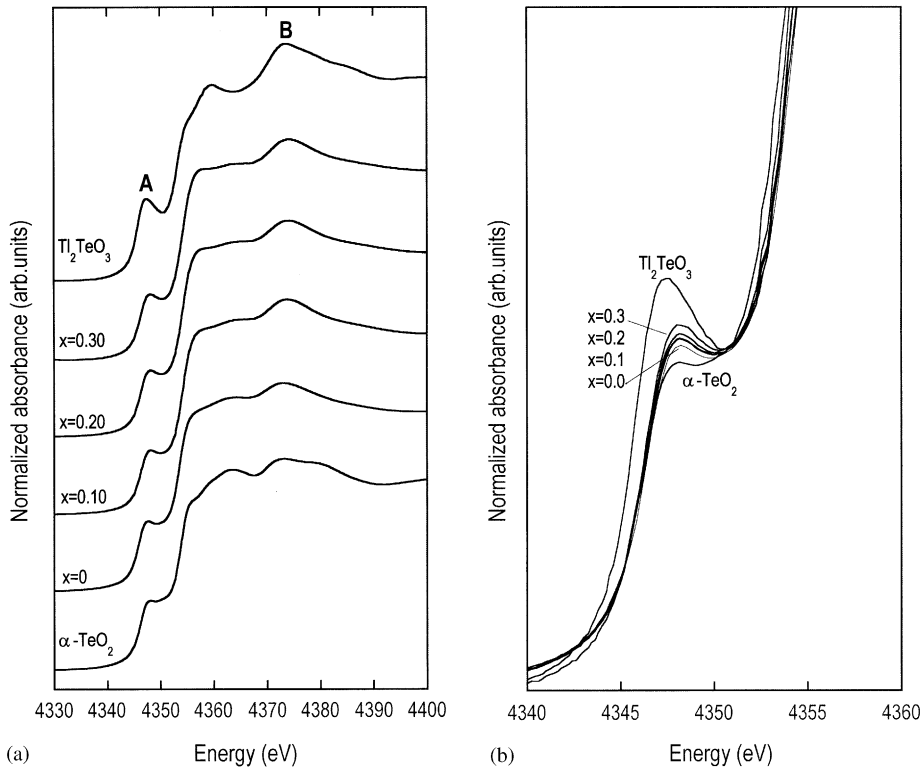

FIG. 2. Normalized Te L_{III} edge XANES spectra of (a) $(1-x)TeO_2$–xWO_3 glasses with the references Tl_2TeO_3 and α-TeO_2. In (b), zoom of the pre-edge feature A.

From a general point of view, Te L_{III} edge XANES data report electronic transitions from the inner Te $2p_{3/2}$ core level to the Te empty states of *s* and *d*-type (30). The form and intensity of the XANES features depend mainly on the density of the vacant states and the transition probability (31). The spectra exhibit a pre-peak, noted A, around 4348 eV, Fig. 2a, characterizing the interactions of the empty Te 5*s* states localized at the bottom of the conduction band with the O $2p_{3/2}$ orbitals (antibonding states) (30, 32). Since the absorption spectra are normalized in the same way, the A pre-peak intensities can be compared, Fig. 2b. The intensity of the pre-peak A depends on the coordination number of the tellurium atoms: it is lower for α-TeO_2 built up from TeO_4E units compared to Tl_2TeO_3 based on pyramidal TeO_3E groups. The same evolution is registered for the resonance feature called B, Fig. 2a, related to the local order around Te atoms (33). The intensity of both the A pre-peak and the feature B increases gradually from TeO_2 glass ($x = 0$) to $x = 0.30$ glass composition, see Figs. 2a and 2b. These increases reveal a continuous change of tellurium atom environment when the WO_3 content increases. From the direct comparison with the crystallized references, it appears that some Te atom sites in $(1-x)TeO_2$–xWO_3 glasses change progressively from TeO_4E (α-TeO_2) to TeO_3E (Tl_2TeO_3) units.

3.3. X-Ray Photoelectron Spectroscopy (XPS)

In order to get structural information from XP spectra, we have compared the core binding energies of the glass samples with those of standard compounds. The core electron binding energy is influenced by the local electron density surrounding the atom and by the structural arrangement of the other atoms within the solid. This is usually referred to as a chemical shift (34). Table 1 reports both the W4$f_{7/2}$ and O1*s* binding energies of glasses and several references. The experimental binding energies are determined with an uncertainty of ± 0.1 eV.

Spectra of the W4f energy region of $(1-x)TeO_2$–xWO_3 glass compositions with $x = 0.05$ and 0.30 and crystallized

TABLE 1
Peak's Position Used by Bigey *et al.* for the Fitting Procedure of XPS Spectra (36)

Oxidation states of tungsten	Binding energies of W $4f_{7/2}$ state (eV)
W^{6+}	35.5
W^{5+}	34.5
W^{4+}	32.7
W^0	31.2

TABLE 2

O1*s* and W4*f* Binding Energies and Full-Widths at Half-Maximum FWHM (in Parentheses) for Some Glass Compositions and Several References

Sample	O1*s* (eV)	W4$f_{7/2}$ (eV)
α-TeO_2	530.6	
	(1.2)	
γ-WO_3	530.7	35.8
	(1.2)	(1.0)
β-$PbWO_4$	530.7	35.4
	(1.1)	(1.0)
TeO_2	530.4	
($x = 0$)	(1.50)	35.8
$0.95TeO_2$–$0.05WO_3$	530.8	(1.2)
($x = 0.05$)	(1.5)	
$0.70TeO_2$–$0.30WO_3$	530.7	35.7
($x = 0.30$)	(1.4)	(1.1)

references β-$PbWO_4$ and γ-WO_3 are presented in Fig. 3a in terms of the W4$f_{7/2}$-4$f_{5/2}$ spin-orbit components. The important information deduced from this analysis concerns the valence state of the W ions in the glasses. Indeed, a large chemical shift is observed for W atoms with 0, +4, +5 and +6 formal oxidation states (36–35), Table 1. The spectra reveal that W^{6+}, characterized by a W4$f_{7/2}$ binding energy at 35.6 ± 0.2 eV (35) similar to this published by Bigey *et al.* (36) (Table 1), constitutes the only oxidation state present in the glasses whatever the composition. Moreover, no signal corresponding to W^{5+} oxidation state was detected by EPR spectroscopy. The W4$f_{7/2}$ binding energy registered for the glasses is closer to that found in γ-WO_3 (WO_6 units) than in β-$PbWO_4$ (WO_4 units), Table 2.

Figure 3b shows O1*s* core-level photoelectron spectra obtained for various glasses and crystallized references. For the crystallized references, the O1*s* peaks consist of only a single and symmetric Gaussian–Lorentzian peak with a small FWHM ≈ 1.2 eV. For $(1-x)TeO_2$–xWO_3 glasses with $x = 0.05$ and 0.30, the registered FWHM of the only one component O1*s* peak is slightly larger, ≈ 1.5 eV, and is independent of glass compositions, Table 1. Himei *et al.* (37) registered the O1*s* binding energies of two references α-TeO_2 (Te–O–Te bridging oxygen atoms, BO) and Li_2TeO_3 (Te–O^-…$^+$Li non-bridging oxygen atoms, NBO). The difference of the O1*s* binding energy between BO (α-TeO_2, 530.5 eV) and NBO (Li_2TeO_3, 529.6 eV) is sufficiently large (0.9 eV) to be registered at least as an asymmetry of the O1*s* peak and an increase of the FWHM (37, 38).

The O1*s* binding energies found for the glass samples are assigned to the existence of bridging oxygen atoms *X*–O–*X* (*X* = Te, W) as found in the registered references, Table 1. Furthermore, the absence of both an asymmetry on the

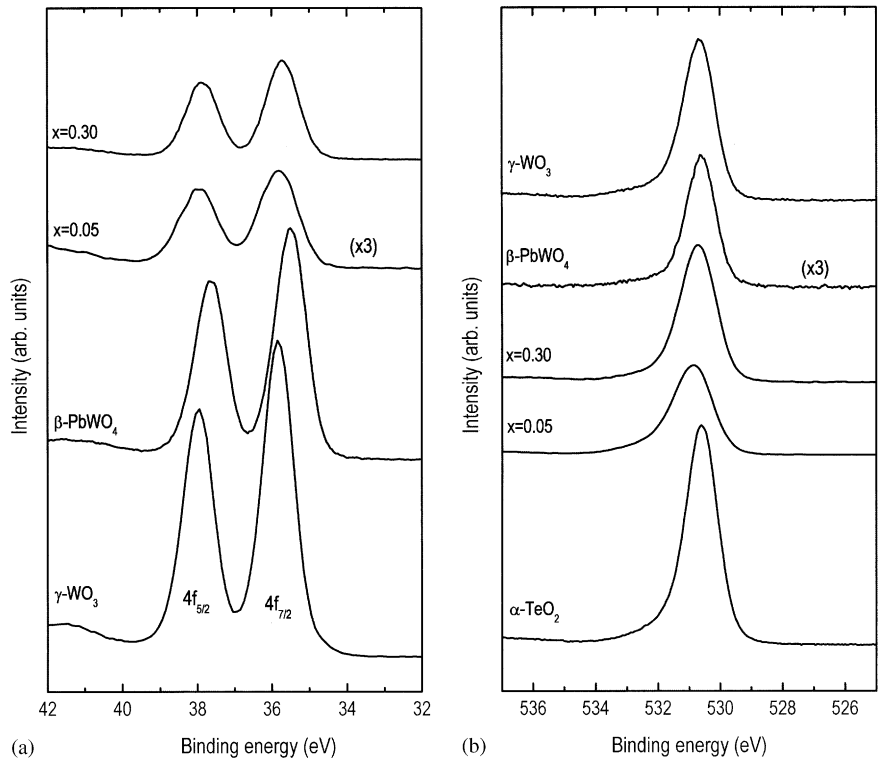

FIG. 3. X-ray photoelectron spectra of (a) the W4f region and (b) the O1*s* core-level photoelectron peak of $x = 0.05$ and 0.30 glass compositions compared with several references.

lower energy side of the O1*s* peak and a shift of the O1*s* peak toward smaller binding energy with increase in the WO_3 content, Fig. 3b, might indicate that oxygen atoms in $(1-x)TeO_2$–xWO_3 glasses with $0.0 \leq x \leq 0.325$ are present only as BO atoms. The shift to higher energy, Table 1, of the O1*s* binding energy in the glasses from $x = 0$ (530.4 eV) to $x = 0.05$ (530.8 eV) and $x = 0.30$ (530.7 eV) could be explained by a difference in the local electron density surrounding the oxygen atoms. TeO_2 glass ($x = 0$) would contain di-coordinated bridging oxygen atoms forming Te–O–Te linkages as in α-TeO_2, while $x = 0.05$ and 0.30 glasses would form Te–O–Te, Te–O–W and W–O–W linkages.

3.4. *W L_{III} and L_I Edges XANES Spectroscopy*

Figure 4a shows the normalized W L_{III} edge XANES signals of crystalline compounds taken as references. The so-called "white line" (WL) resonance, labeled A, corresponds to the dipole-allowed transition from the $2p_{3/2}$(W) core level to a quasi-bound 5d(W) + 2*p*(O) mixed-state (39). The amplitude of the WL is larger in γ-WO_3 reference compared to $Li_2W_2O_7$, both structures are built up with distorted WO_6 octahedra. In stoichiometric γ-WO_3 and $Li_2W_2O_7$, the tungsten ions have the valence state 6+ with an empty 5*d* shell. The decrease of the WL intensity is due to the increase of distortion of WO_6 octahedra (40). The sharp, fairly intense post-edge feature B registered only for $BaWO_4$ spectrum is characteristic of WO_4 tetrahedra.

Normalized W L_{III} edge XANES spectra of $(1-x)TeO_2$–xWO_3 glasses with $0.10 \leq x \leq 0.30$ are presented in Fig. 4b. The shape of the absorption spectra undergoes no considerable changes with x. The absence of a post-edge feature B, as encountered in $BaWO_4$, shows that the W environment in the glasses consists only in WO_6 octahedra. Furthermore, the significant decrease of the amplitude of the WL registered from $x = 0.10$ to 0.30 suggests an increase of the WO_6 octahedra distortion with the WO_3-content.

We present in Fig. 5a the normalized XANES regions registered at W L_I edge for three references, γ-WO_3, $Li_2W_2O_7$ and $BaWO_4$. The intensity of the pre-edge feature A observed in W L_I edge XANES spectra is determined primarily by the site symmetry of the transition-metal ion. Indeed, the electronic transition $2s(W) \rightarrow 5d(W) + 2p(O)$ is dipole forbidden in the case of regular octahedra (inversion center), but is allowed for distorted octahedra and tetrahedra (39, 41). The amplitude of the pre-edge feature A is the largest in the case of W tetrahedral coordination ($BaWO_4$) and is registered as a weak shoulder for distorted W octahedra (γ-WO_3 and $Li_2W_2O_7$). Furthermore, its amplitude depends on the degree of WO_6 octahedra

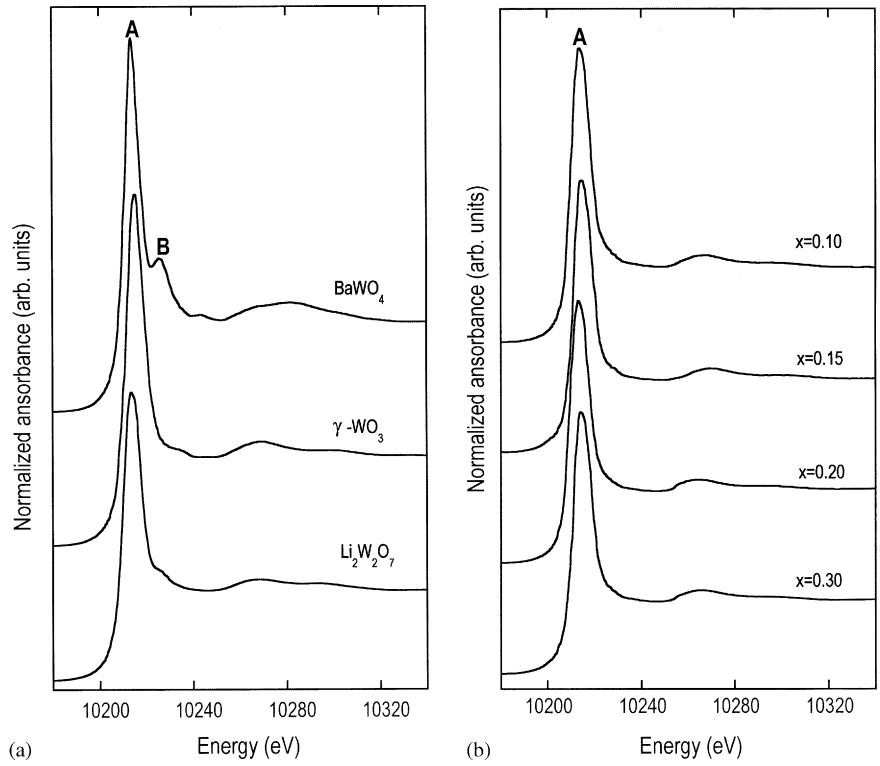

FIG. 4. Normalized W L_{III} edge XANES spectra of (a) the crystallized references $BaWO_4$, γ-WO_3 and $Li_2W_2O_7$ and of (b) $(1-x)TeO_2$–xWO_3 glasses.

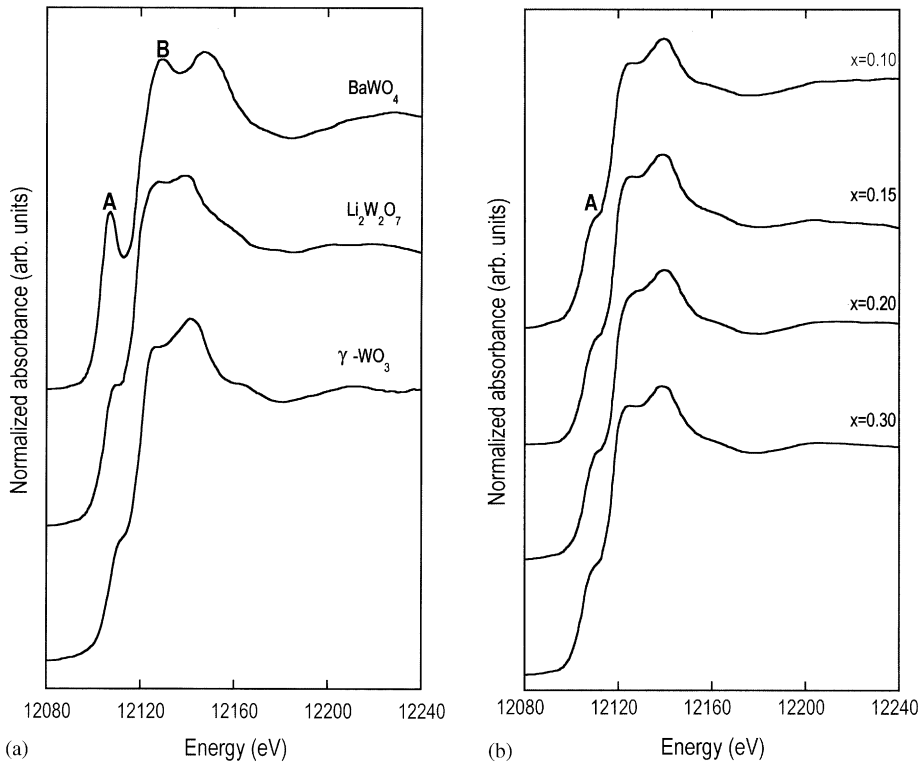

FIG. 5. Normalized W L_I edge XANES spectra of (a) the crystallized references $BaWO_4$, γ-WO_3 and $Li_2W_2O_7$ and of (b) $(1-x)TeO_2$–xWO_3 glasses.

distortion. Indeed, the distortion of the octahedra facilitates $d-p$ orbital mixing, and thus enhances the pre-edge feature A amplitude (40). The pre-edge feature A has the largest amplitude in $Li_2W_2O_7$ compared to γ-WO_3 reference in accordance with the increase of the average W–O bond length from 1.926 to 1.955 Å. The edge feature, labeled B, is the allowed dipole transition $2s(W) \rightarrow 6p(W) + 2p(O)$ (40).

Normalized W L_I edge XANES spectra of $(1-x)TeO_2$–xWO_3 with $0.10 \leq x \leq 0.30$ are presented in Fig. 5b. The shape of the absorption spectra undergoes no considerable changes with x and present close similitude with the spectrum of the reference γ-WO_3. The pre-edge feature A is present as a shoulder indicating the presence of distorted WO_6 octahedra site in these glasses as pointed out by the W L_{III} edge XANES analysis.

4. DISCUSSION

The glass transition temperatures, Tg, registered for glasses obtained in the TeO_2–WO_3 system increase regularly with the WO_3 content (1, 5). This compositional dependence of Tg can reveal a transformation of the glass structure referred to the increase in the network connectivity. The presence of tungsten atoms would lead to a densification of the TeO_2 glass matrix. The IR curves of the $(1-x)TeO_2$–xWO_3 glasses with $0 \leq x \leq 0.325$ clearly show a regular evolution of their shape with x in accordance with the Tg evolution. The analysis of these IR data shows the formation of Te–O–W linkages that contribute to the Tg increases (9) and an evolution of the Te surrounding. Indeed, the trigonal bipyramid TeO_4E units forming TeO_2 ($x = 0$) glass are the major components of the glass network. However, for high WO_3 content, some of these TeO_4E units are converted in trigonal pyramids TeO_3E.

The existence of a mixed Te environment (TeO_4/TeO_3) for glasses with high WO_3 content is also pointed out by Te L_{III} XANES spectroscopy. The main XANES feature registered for $(1-x)TeO_2$–xWO_3 glasses, Fig. 2b, is the pre-peak, A, which corresponds to the $2p \rightarrow 5s$(Te) transition. The regular evolution in the intensity of this pre-peak with x may also be related to the stereochemical activity of the lone pair $5s^2$(Te) (32, 42), that directly depends on the tellurium coordination number. The stereochemical activity of the lone pair $5s^2$(Te) is maximum in the reference Tl_2TeO_3 made up of TeO_3E trigonal pyramids. Thus, the registered evolution of the Te L_{III} XANES spectra with the WO_3 content indicates a progressive transformation of some Te polyhedra from TeO_4E units to more regular TeO_3E units.

This result concerning the structural evolution of the tellurium polyhedra in function of the composition is consistent with other works using Raman spectroscopy (8, 10). On the other hand, most of the papers describing

IR and Raman data on these tungsten oxide–tellurite glasses assumed that Te is only present as TeO_4E units whatever the composition (2, 7, 11). Indeed, the $TeO_4E \rightarrow TeO_3E$ transformation is not clearly observed on Raman spectra, the Te–O bands appearing at the same range as W–O vibrations.

Now concerning the W^{6+} ion coordination state in TeO_2–WO_3 glasses, a large credit is given, in the literature, either to the presence of only WO_4 tetrahedra (2, 11) or to the existence of a mixed W coordination state made of WO_4 tetrahedra and WO_6 octahedra (4, 7, 8, 10). Few papers report on the existence of tungsten ions in six-coordination whatever the glass composition (9).

As pointed out in our IR study, the presence of the band centered at $930\,cm^{-1}$ attributed to W–O vibration is difficult to interpret in terms of WO_4 or WO_6 polyhedra. It is why we have undertaken an X-ray absorption spectroscopy study at the W L_{III} and L_I edges. Indeed, XANES spectroscopy is a powerful tool to provide information on the local symmetry and coordination around a given element. Since W L_{III} and L_I edges XANES features are sensitive to both the W oxidation state and the site geometry, we performed XPS analyses on TeO_2–WO_3 glasses to identify the W oxidation state. Indeed, tungsten oxide is one of the transition metal oxides which have two different oxidation states, namely W^{5+} and W^{6+}. It is known that in tungsten glasses the electric conduction arises from electron hopping between these two oxidation states (43, 44).

Spectra of the W4*f* energy region of $(1-x)TeO_2$–xWO_3 glass compositions with $x = 0.05$ and 0.30 reveal that W^{6+} constitutes the only oxidation state present in the glasses whatever the composition. Based on this result, the registered features on the W L_{III} and L_I edges XANES spectra were analyzed. Both W L_{III} and L_I XANES studies agree with the existence of W^{6+} ions in six-fold coordination whatever the glass composition in agreement with (9). The radius ratio of W^{6+} to O^{2-} indicates that W^{6+} prefers six-coordination (9). Furthermore, the distortion of the WO_6 octahedra increases with the WO_3 content and thus, with the formation of TeO_3E entities. The high distortion of the WO_6 octahedra seems to be responsible for the formation of the $930\,cm^{-1}$ IR band. This $930\,cm^{-1}$ band is present as a sharp peak on Raman spectra and its intensity increases with the WO_3 content (9), i.e., with the WO_6 distortion. The WO_6 octahedra deformation could be to such a degree, that the W atoms may be located in a more or less off-centered position in octahedral site as in the crystal chemistry of tungstates. Then, the distinction between WO_6 and WO_4 units becomes impossible with this single vibrationnal band.

The formation of $X^+ \ldots {}^-O$–Te non-bridging oxygen atoms is not expected in the TeO_2–WO_3 glasses. The O1*s* binding energies found for the glass samples could be assigned to the existence of bridging oxygen atoms *X*–O–*X* (*X* = Te, W). However, the existence of TeO_3E trigonal pyramids with three bridging oxygen atoms brings a local positive charge which has to be compensated. The local electrostatic neutrality of the TeO_3E units could be respected with the formation of a Te–O terminal bond with double bond character (Te = O). The electronic density surrounding Te = O oxygen atoms is relative close to BO atoms. Considering the small Te = O proportion, the contribution of such terminal bonds cannot be distinguished from other oxygen atoms.

5. CONCLUSION

Transparent and stable glasses were obtained in the TeO_2–WO_3 system. Their short range order was approached using several complementary techniques. Infrared and Te L_{III} XANES spectroscopies pointed out the evolution of the Te environment in function of the glass composition. The trigonal bipyramids TeO_4E are the main structural constituents of these glasses. Therefore, when the WO_3 content increases, some trigonal pyramids TeO_3E are formed. Also, some W atoms are incorporated into the glass network to form Te–O–W linkages.

We were very concerned by the oxidation state and the coordination state of the tungsten atoms. For the first time, a precise determination of the W environment in TeO_2–WO_3 glasses was realized by XANES spectroscopy. W^{6+} ions are in six-fold coordination state whatever the glass composition. These WO_6 octahedra present high distortion that increases with the WO_3 content, i.e., with the glass network deformation.

REFERENCES

1. T. Kosuge, Y. Benino, V. Dimitrov, R. Sato, and T. Komatsu, *J. Non-Cryst. Solids* **242,** 154 (1998).
2. I. Shaltout, Y. Tang, R. Braunstein, and E. E. Shaisha, *J. Phys. Chem. Solids* **57,** 1223 (1996).
3. S. K. J. Al-Ani, C. A. Hogarth, and R. A. El-Malawany, *J. Mater. Sci.* **20,** 661 (1985).
4. V. Kozhukharov, M. Marinov, and G. Grigorova, *J. Non-Cryst. Solids* **28,** 429 (1978).
5. S. Blanchandin, P. Marchet, P. Thomas, J.-C. Champarnaud-Mesjard, B. Frit, and A. Chagraoui, *J. Mater. Sci.* **34,** 4285 (1999).
6. V. Kozhukharov, S. Neov, I. Gerasimova, and P. Mikula, *J. Mater. Sci.* **21,** 1707 (1986).
7. V. Dimitrov, M. Arnaudov, and Y. Dimitriev, *Monatsh. Chem.* **115,** 987 (1984).
8. M. Tatsumisago, T. Minami, Y. Kowada, and H. Adachi, *Phys. Chem. Glasses* **35,** 89 (1994).
9. T. Sekiya, N. Mochida, and S. Ogawa, *J. Non-Cryst. Solids* **176,** 105 (1994).
10. B. V. R. Chowdari and P. Pramoda Kumari, *Mater. Res. Bul.* **34,** 327 (1999).

11. I. Shaltout, Y. Tang, R. Braunstein, and A. M. Abu-Elazm, *J. Phys. Chem. Solids* **56,** 141 (1995).
12. S.-H. Kim, T. Yoko, and S Sakka, *J. Am. Ceram. Soc.* **76**(10), 2486 (1993).
13. S. Blanchardin, P. Marchet, P. Thomas, J. C. Champarnaud-Mesjard, B. Frit, and A. Chagraoui, *J. Mater. Sci.* **34,** 4285 (1999).
14. P. A. Thomas, *J. Phys. C* **21,** 4611 (1988).
15. B. O. Loopstra and P. Boldrini, *Acta Crystallogr.* **21,** 158 (1966).
16. K. Okada, H. Morikawa, F. Marumo, and S. Iwai, *Acta Crystallogr. B* **31,** 1451 (1975).
17. E. Gürmen, E. Daniels, and J. S. King, *J. Chem. Phys.* **55,** 1093 (1971).
18. J. M. Moreau, Ph. Galez, J. P. Peigneux, and M. V. Korzhik, *J. Alloys Compd.* **238,** 46 (1996).
19. P. Sainctavit, J. Petiau, A. Manceau, R. Rivallant, M. Belakhovsky, and G. Renaud, *Nucl. Instrum. Methods* **273,** 423 (1988).
20. D. A. Shirley, *Phys. Rev. B* **5,** 4709 (1972).
21. M. Arnaudov, V. Dimitrov, Y. Dimitriev, and L. Markova, *Mater. Res. Bull.* **17,** 1121 (1982).
22. G. M. Clark and W. P. Doyle, *Spectrochim. Acta* **22,** 1441 (1966).
23. T.Yoko, K. Kamiya, K. Tanaka, H. Yamada, and S. Sakka, *Nippon Seram. Kyo. Gakuj. Ronb.* **97,** 289 (1989).
24. Y. Dimitriev, V. Y. Dimitrov, V. Dimitrov, and M. Arnaudov, *J. Mater. Sci.* **18,** 1353 (1983).
25. Y. Mizuno, M. Ikeda, and A. Yoshida, *J. Mater. Sci. Lett.* **11,** 1653 (1992).
26. A. Miller, K. Nassau, K. Lyons, and M. Lines, *J. Non-Cryst. Solids* **99,** 289 (1988).
27. S. Muthupari and K. J. Rao, *J. Phys. Chem. Solids* **57,** 553 (1996).
28. P. Caillet and P. Saumagne, *J. Mol. Structure* **4,** 191 (1969).
29. B. Frit, D. Mercurio, P. Thomas, and J.-C. Champarnaud-Mesjard, *Z. Kristallogr. NCS* **214,** 439 (1999).
30. P.-E. Lippens, J. Olivier-Fourcade, J.-C. Jumas, A. Gheorghiu, S. Dupont, and C. Sénémaud, *Phys. Rev. B* **56,** 13057 (1977).
31. M. Marezio and J. P. Remeika, *J. Chem. Phys.* **46,** 1862 (1967).
32. J.-C. Sabadel, P. Armand , P.-E. Lippens, D. Cachau-Hereillat, and E. Philippot, *J. Non-Cryst. Solids* **244,** 143 (1999).
33. A. Ibanez, T. Ericsson, O. Lindqvist, D. Bazin, and E. Philippot, *J. Mater. Chem.* **4,** 101 (1994).
34. G. E. McGuire, G. K. Schweitzer, and T. A. Carlson, *Inorg. Chem.* **12,** 2450 (1973).
35. R. J. Colton and J. W. Rabalais, *Inorg. Chem.* **15,** 236 (1976).
36. C. Bigey, V. Logie, A. Bensaddik, J. L. Schmitt, and G. Maire, *J. Phys. IV France* **8,** Pr5-553 (1998).
37. Y. Himei, Y. Miura, T. Nanba, and A. Osaka, *J. Non-Cryst. Solids* **211,** 64 (1997).
38. Y. Miura, H. Kusano, T. Nanba, and S. Matsumoto, *J. Non-Cryst. Solids* **290,** 1 (2001).
39. A. Kuzmin and J. Purans, *J. Phys. IV France* **7,** C2-971 (1997).
40. A. Balerna, E. Bernieri, E. Burattini, A. Kuzmin, A. Lusis, J. Purans, and P. Cikmach, *Nucl. Inst. Methods Phys. Res. A* **308,** 240 (1991).
41. J. A. Horsley, I. E. Wachs, J. M. Brown, G. H. Via, and F. D. Hardcastle, *J. Phys. Chem.* **91,** 4014 (1987).
42. J. Olivier-Fourcade, A. Ibanez, J.-C. Jumas, H. Dexpert, C. Blancard, J.-M. Esteva, and R. C. Karnatak, *Eur. J. Solid State Inorg. Chem.* **28,** 409 (1991).
43. A. A. Bahgat, M. M. El-Samanoudy, and A. I. Sabry, *J. Phys. Chem. Solids* **60,** 1921 (1999).
44. C. A. Hogarth and E. Assadzadeh-Kashani, *J. Mater. Sci.* **18,** 1255 (1983).